Downloaded from UvA-DARE, the institutional repository of the University of Amsterdam (UvA)
http://dare.uva.nl/document/104845

File ID	104845
Filename	7 Charm cross-sections

SOURCE (OR PART OF THE FOLLOWING SOURCE):

Type	Dissertation
Title	Measurement of charm production in deep inelastic scattering at HERA II
Author	T.G. Grigorescu
Faculty	Faculty of Science
Year	2008
Pages	vi, 168
ISBN	9789064880308

FULL BIBLIOGRAPHIC DETAILS:
http://dare.uva.nl/record/271134

Copyright

It is not permitted to download or to forward/distribute the text or part of it without the consent of the author(s) and/or copyright holder(s), other then for strictly personal, individual use.

UvA-DARE is a service provided by the library of the University of Amsterdam (http://dare.uva.nl)

Chapter 7

Charm cross-sections

In this chapter, the measurements of events containing an untagged D^0 meson (not coming from a D^* decay) in the final state are presented. The charm cross-sections are presented as functions of photon virtuality Q^2 of the event, transverse momentum P_T of the charm meson, pseudo-rapidity η of the charm meson and Bjorken x. The kinematic region has been chosen such that the results can be compared to previous ZEUS measurements performed on HERA I data.

7.1 Definition of the cross-sections

The measured cross-sections are $d\sigma/dQ^2$, $d\sigma/dP_T(D^0)$, $d\sigma/d\eta(D^0)$ and $d\sigma/dx$. The measurement was performed in the following kinematic region:

- $5\,\mathbf{GeV^2} < Q^2 < 1000\,\mathbf{GeV^2}$
- $0.02 < y < 0.7$
- $3 < P_T(D^0) < 20\,\mathbf{GeV}$

As the measurement required a D^0 meson in the final state which did not come from a D^* decay as the only criterion, the cross-sections include events both involving direct charm decay or charm decay that followed from a beauty meson decay.

The differential cross-section $d\sigma/d\alpha$ for a given observable α was computed as:

$$\frac{d\sigma}{d\alpha} = \frac{N^{data}}{\mathcal{A}\,\mathcal{L}\,\mathcal{B}\,\Delta\alpha} \tag{7.1}$$

where $\mathcal{A}$ is the acceptance in the corresponding α bin, $\mathcal{L}$ is the total luminosity of the data set, $\mathcal{B}$ is the branching ratio for the particular decay channel and $\Delta\alpha$ is

the bin width. The 2005 e^-p data set has a luminosity of $\mathcal{L} = 127.35\,\mathbf{pb^{-1}}$. The branching ratio quoted by the Particle Data Group in 2006 for the $D^0 \to K^- + \pi^+$ decay is $\mathcal{B} = 3.82 \pm 0.07\%$. The detector acceptance $\mathcal{A}$ within a given bin $\Delta\alpha$ was determined from Monte Carlo as the ratio between the number of reconstructed candidates and the number of generated mesons within that bin: $\mathcal{A} = N^{recon}/N^{gen}$ and also includes effects of bin to bin migration.

7.2 Systematic uncertainties

To accurately account for the errors induced by the uncertainties on variables used to select the final event sample, the thresholds of various cuts were varied both to larger and smaller values within the resolution of these variables. This was done both in data and Monte Carlo. The variations on individual cuts are listed in Table 7.1. For some variables, the threshold can be varied only in one direction: varying

Variable	Nominal Thres.	Variation
$z_{vtx}(\mathbf{cm})$	30	± 5
$E - P_Z(\mathbf{GeV})$	$40 - 65$	$\to 45 - 60$
$E(e^-)(\mathbf{GeV})$	10	$\to 11$
$Y_{el.}$	0.95	$\to 0.9$
Y_{JB}	0.02	$\to 0.03$
Box Cut ($\mathbf{cm^2}$)	15×15	$\to 16 \times 16$
MVD Hits (K)	2	$\to 3$
MVD Hits (π)	2	$\to 3$
$P_T(K)(\mathbf{GeV})$	0.8	± 0.1
$P_T(\pi)(\mathbf{GeV})$	0.8	± 0.1
$\lvert\eta(K)\rvert$	1.6	± 0.05
$\lvert\eta(\pi)\rvert$	1.6	± 0.05
$\chi^2_{sec}/ndof$	8	± 1
$\sigma(D.L.)$	1	$\uparrow 2$ and $\downarrow -1$

Table 7.1. List of cuts which generate systematic uncertainties. The nominal thresholds and their variations are shown. For certain variables, variations in only one direction were allowed; the resulting systematic error in these cases were symmetrized.

in the opposite direction would spoil the data set by allowing background events into the sample. To fully take into account the effects of the cut variations, a

detailed description of the background would be necessary. When this is the case, the obtained error is symmetrized.

A nominal cross-section σ_0 is calculated, corresponding to the nominal cuts. Each variation of a given variable i leads to a new cross-section value σ_i . Defining $\delta_i = \sigma_i - \sigma_0$, the upper and lower systematic errors Δ_i^+ and Δ_i^- on the cross-section due to source i are computed as:

$$\Delta_i^+ = \begin{cases} \delta_i \ \ if \ \ \delta_i > 0 \\ 0 \ \ if \ \ \delta_i < 0 \end{cases}$$

$$\Delta_i^- = \begin{cases} \delta_i \ \ if \ \ \delta_i < 0 \\ 0 \ \ if \ \ \delta_i > 0 \end{cases}$$

The total error is then computed by summing all the individual errors in quadrature:

$$\Delta^+ = \sqrt{\sum_i (\Delta_i^+)^2} \tag{7.2}$$

and

$$\Delta^- = \sqrt{\sum_i (\Delta_i^-)^2} \tag{7.3}$$

The systematic error induced by each of the variations from Table 7.1 are shown as a function of Q^2, $P_T(D^0)$, $\eta(D^0)$ and x in Fig. 7.9, 7.10, 7.11 and 7.12. These errors will be discussed in detail below.

7.2.1 DIS selection

The errors due to the DIS selection are small with respect to other sources. To account for these errors, the z_{vtx} of the primary vertex, $E - P_z$, the electron energy, Y_{JB} and Y_{el}, as well as the box cut around the beam pipe were varied. A significant contribution came from the box cut variation at low Q^2 (the electron hits the RCAL closer to the beampipe at low Q^2). The shift between the data and the Monte Carlo electron energy displayed by control plots in Fig. 6.12 also introduces a noticeable systematic error. The size of these errors is estimated to be $\sim 5\%$.

7.2.2 Track momentum and pseudo-rapidity

The uncertainty in track momentum was accounted for by varying the momenta of both the kaon and the pion tracks by $\pm 0.1\,\mathbf{GeV}$. The effect on the final cross-section was negligible. The pseudo-rapidity cut was also varied by ± 0.05 units for both tracks. This effect was less than 8%, despite the slight disagreement in pseudo-rapidity seen in control plots in Fig. 6.13.

7.2.3 Uncertainty in the MC beauty fraction

In addition to charm mesons directly produced at the interaction point, the simulated sample contains a small number of charm candidates coming from beauty meson decays. In total, 1147 *true* D^0 generated mesons originated from beauty meson decays, compared to 33679 D^0 mesons generated at the interaction point. Both numbers correspond to an equivalent luminosity of $295\,pb^{-1}$. The charm mesons originating from beauty decay form *the beauty fraction*. In order to determine how sensitive the measurement is to the beauty fraction, the Monte Carlo beauty fraction was doubled and its induced error on the cross-section symmetrized. The effect was not significant with respect to other error sources, indicating that the measurement is not sensitive to beauty production.

7.2.4 Luminosity

The luminosity at ZEUS, for the 2005 data set, is known within 2 % accuracy. This error is not added to the total systematic error.

7.2.5 Number of MVD hits

The control plots in Fig. 6.13 revealed that in the Monte Carlo more signal events are reconstructed where both the K and the π daughter tracks have more hits in the MVD when compared to tracks in the data. This is a known flaw of the Monte Carlo and it is caused by some dead strips in the MVD not being simulated in Monte Carlo. Therefore, the simulation contains relatively more tracks, on the average, with a higher number of MVD hits. In this analysis, a minimum of 2 hits in the MVD was required for both the K and the π. The systematic error due to this cut was computed by changing the threshold to 3 hits for each of the two tracks. This error is significant and is at the level of 5%.

7.2.6 Signal extraction

A significant statistical error appears in the final cross-section measurement due to the signal extraction. The systematic error associated with signal extraction has also been investigated. In particular, due to the fact that the Monte Carlo does not contain light flavor decays, the signal over background ratio is much enhanced in Monte Carlo. This leads to an inaccurate modeling of the background w.r.t. the data sample. The fit for extracting the number of candidates is performed by the MINUIT package [44] within ROOT. The fit function is given in Eq. 6.1. As a systematic variation, the background component of the function was changed to a linear function. The error introduced by changing the background function is not significant, being at the level of 2-3% for most of the bins.

7.2.7 Reflected signal subtraction

Wrong mass assignment to the daughter track pair pollutes the signal. An iterative procedure of subtracting the reflected signal was explained in detail in Chap. 6. Despite the fact that the procedure is applied independently in data and in the Monte Carlo, significant errors are introduced because statistical fluctuations are scaled up during the iterative process. To account for this effect, all cross-sections were recomputed without subtracting the reflected signals for any of the fits. The errors were symmetrized. Although in some bins the errors reach the 10-15% level, especially in the η bins, they are within the statistical errors.

7.2.8 Uncertainty due to the D.L. significance

Tagging the charmed meson decay and using decay related variables to enhance the charm purity of the sample is another source of systematic errors. When comparing data with simulation, as in Fig. 6.14, an overall good agreement is seen for the entire spectrum of variables such as χ^2 of the secondary vertex and the signed decay length itself. A disagreement is seen when comparing the data and simulated signals in bins of the decay length error, namely there are relatively more candidates in the Monte Carlo with small decay length errors. Errors are underestimated in the Monte Carlo for various reasons: inappropriate treatment of dead material, alignment issues, dead cells in the MVD or noisy detector cells not correctly accounted for and so on. Therefore, event selection by decay significance has a strong dependence on the decay length error. This is investigated further.

One defines the signal efficiency associated with the decay length significance cut as:

$$\epsilon = \frac{N_\sigma}{N_R} \tag{7.4}$$

where N_σ is the number of signal candidates at a minimal particular decay significance cut σ_{DL} and N_R is a reference signal, extracted without a significance cut. In Fig. 7.1, the signal efficiency in data and Monte Carlo are compared. Differences are visible. The relative data efficiency ϵ_{rel}, defined below, quantifies these differences.

$$\epsilon_{rel} = (\epsilon_{data} - \epsilon_{MC})/\epsilon_{MC} \tag{7.5}$$

ϵ_{rel} is also shown in Fig. 7.1. The simulation describes well the data up to a decay

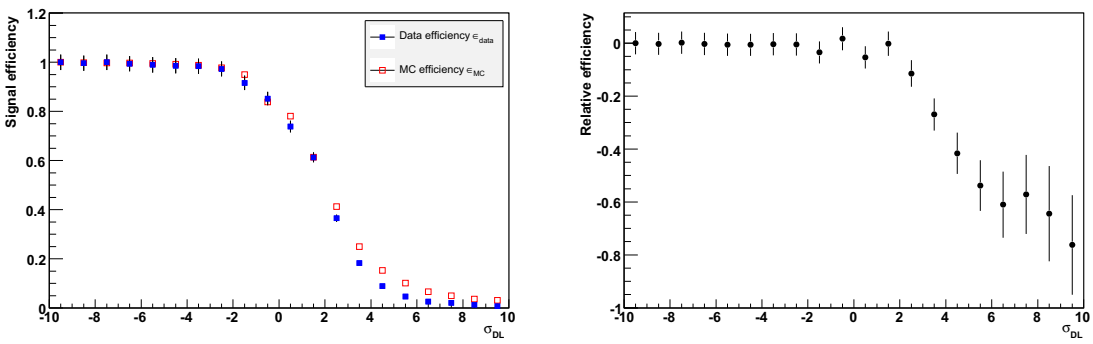

Figure 7.1. Left plot: Signal efficiency as a function of the D.L. significance cut, comparison between data, in colored squares, and Monte Carlo, in open squares. Right plot: The relative difference of the two efficiencies as defined in Eq. 7.5.

significance of $\sigma_{DL} = 2$ which is larger than the nominal cut used in this analysis. As the significance has per definition a pull of 1 and because the nominal significance cut is within the range for which the Monte Carlo describes the data, thresholds of one unit away from the nominal value, $\sigma_{DL}^{low} = 0$ and $\sigma_{DL}^{high} = 2$, can be used for calculating the systematic error.

A more conservative approach can be taken. The efficiency ϵ was plotted in Fig. 7.2 as a function of decay length error Δ_{DL}, both for data and for Monte Carlo. The right plot denotes the relative difference between the data and the simulated sample efficiencies. An overall variation of 75% in the relative efficiency difference can be seen (in one direction only) when the entire decay length error spectrum is spanned.

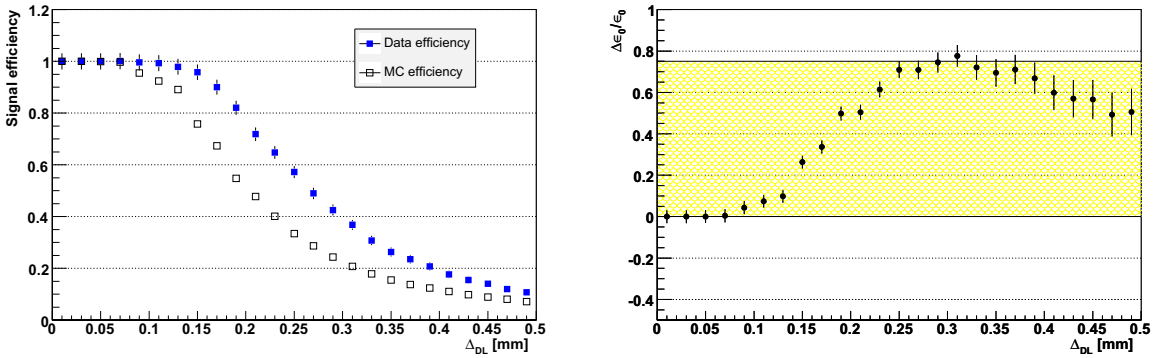

Figure 7.2. Left plot: signal efficiency in data (solid squares) and MC (open squares) as a function of decay length error Δ_{DL}. Right plot: the relative difference of the two signal efficiencies. An overall variation of 75 % in relative efficiency difference is sufficient within the errors to contain the entire efficiency spectrum.

The efficiency variation extracted from the decay length error spectrum in Fig. 7.2 is propagated to the efficiency plot in Fig. 7.3. The horizontal shaded area denotes the 75% efficiency error which has been centered on the nominal cut of $\sigma_{DL} = 1$. A modified arc-tangent function, fitted along the efficiency slope, reaches the outer edges of the error band at of $\sigma_{DL}^{low} = -1$ and $\sigma_{DL}^{high} = 2$. These are the variational thresholds employed in this analysis for calculating the induced systematic error. In conclusion, both the "one unit away from the nominal value" rule and the conservative approach taken above lead to very similar estimates for the variation of the D.L. significance employed in calculating the systematic error. This is confirmed by the fact that the simulation and the data agree well in efficiency for all values of D.L. significance below $\sigma_{DL} = 1$, as shown in Fig. 7.1 (right plot) and that the number of candidates in the region of disagreement, in relation to the total number of candidates, is minute.

It is worth mentioning that a solution for reducing significantly the systematic errors due to σ_{DL} can be found by rescaling the decay length error in the Monte Carlo such that it describes the data as accurately as possible. As an exercise, a simple rescaling of the form $\Delta_{DL}^{new} = 120\%\Delta_{DL}$ was performed only on the simulated samples. The new relative efficiency difference is plotted once more in Fig. 7.4. Only a 20% variation in relative efficiency difference is seen after scaling up the Monte Carlo decay length error. This could be improved further.

The decay significance systematic error contributes the most to the final error with respect to any other sources. Nevertheless, this error is comparable to the

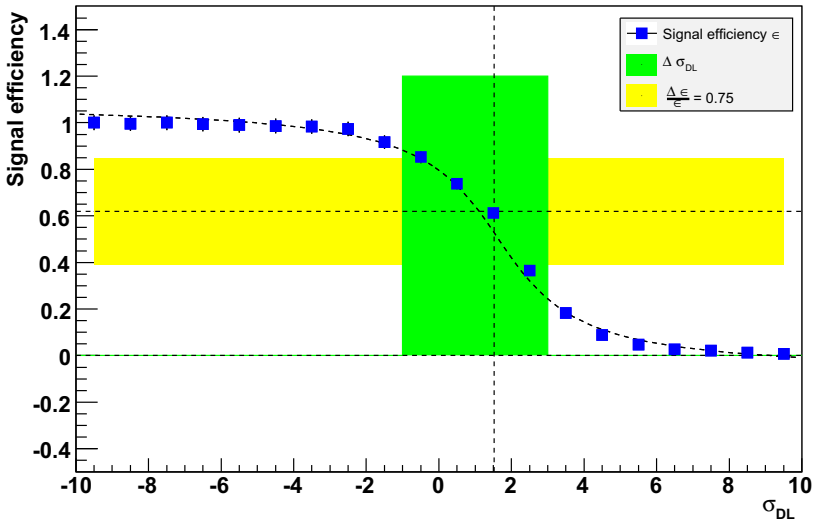

Figure 7.3. The signal efficiency in data as a function of the decay length significance is shown in solid squares. The nominal cut used in this analysis is $\sigma_{DL} = 1$. An arc-tangent function is fitted to the efficiency curve. The horizontal shaded band centered on the nominal cut represents the 75 % variation in relative efficiency extracted from the decay length error spectrum (see Fig. 7.2). A systematic shift in reconstructing σ_{DL} by $\pm\Delta\sigma_{DL}$ is equivalent to a systematic shift in the signal efficiency. Therefore, a variation in significance is computed. The arc-tangent fit intersects the outer edges of the horizontal shaded error band at $\sigma_{DL}^{low} = -1$ and at $\sigma_{DL}^{high} = 2$. These are the two σ_{DL} up and down threshold values used to compute the systematic errors induced by the decay length tag.

statistical error of the measurement.

7.3 D^0 cross-sections

7.3.1 Differential cross-section w.r.t. Q^2: $d\sigma/dQ^2$

The differential cross-section w.r.t. the photon virtuality Q^2 of the event for the process $e^-p \to e^- + D^0 + X$ has been measured for the bins: $Q^2 \in \{5, 15, 40, 100, 1000\}$ **GeV²**. The results are presented in Fig. 7.5 and tabulated in Appendix B, Table B.1. The inner error bars (where visible) denote the statistical errors, the outer error bars represent the systematic errors. The measurement is compared to a second ZEUS analysis performed recently by John Loizides and Dan Nicholass from University College London. The second analysis measured within the same kinematic range as the one defined in Sec. 6.3 but was performed independently, using different tracking and vertexing packages, a slightly larger data set and some different cleaning

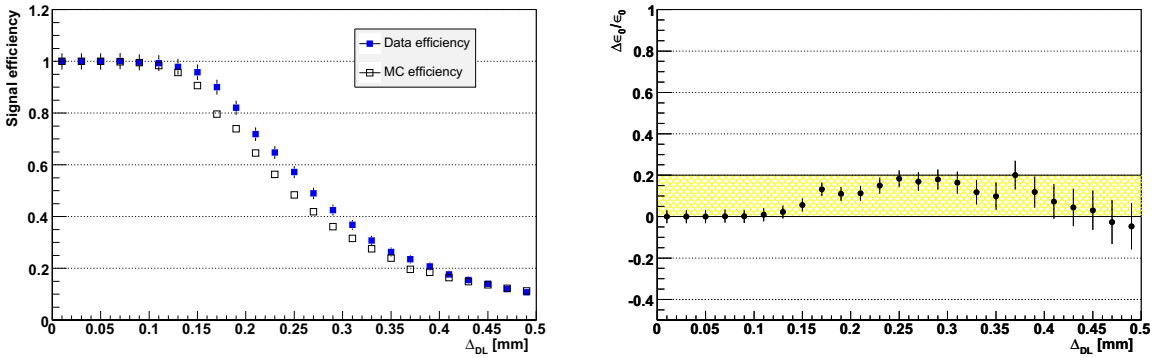

Figure 7.4. Left plot: signal efficiency in data (solid squares) and simulation (open squares) as a function of decay length error Δ_{DL}, after rescaling the Monte Carlo decay length error by a 20% increase. Right plot: the new relative difference of the two signal efficiencies. An overall variation of only 20 % in relative efficiency difference is seen after rescaling.

cuts. The results of a previous ZEUS measurement, using HERA I data [47], are also shown, for the first two Q^2 bins only. The next to leading order theoretical prediction is also displayed, together with its error. Details on how the NLO prediction was calculated are given in Sec. 7.4. The relative difference between the measurement and the theoretical prediction, as defined in Eq. 7.6, is shown separately (bottom plot). The error bars correspond to the relative total error (statistic and systematic); the shaded band is the relative error of the theoretical prediction. There is good agreement in shape between the data and the theoretical prediction but the overall normalization is off by $\sim 15-25\%$. The systematic errors on $d\sigma/dQ^2$ due to the sources listed in Table 7.1 are displayed in Fig. 7.9. The total systematic error (lower plot in Fig. 7.9) is calculated by adding all systematic errors in quadrature. It is worth mentioning that for each systematic variation, the signal extraction is subject to a statistical fit error which cannot be decoupled from the intrinsic systematic error. Therefore, low statistics bins, such as the high Q^2 bin, display larger systematic errors due to the fact that the background and signal fits suffer from statistical fluctuations.

7.3.2 Differential cross-section w.r.t. $P_T(D^0)$: $d\sigma/dP_T$

The differential cross-section as a function of the charm meson transverse momentum $P_T(D^0)$ for the process $e^-p \to e^- + D^0 + X$ has been measured for the following bins: $P_T \in \{3, 3.5, 4.5, 6, 20\}$ **GeV**. The results are presented in Fig. 7.6 and tab-

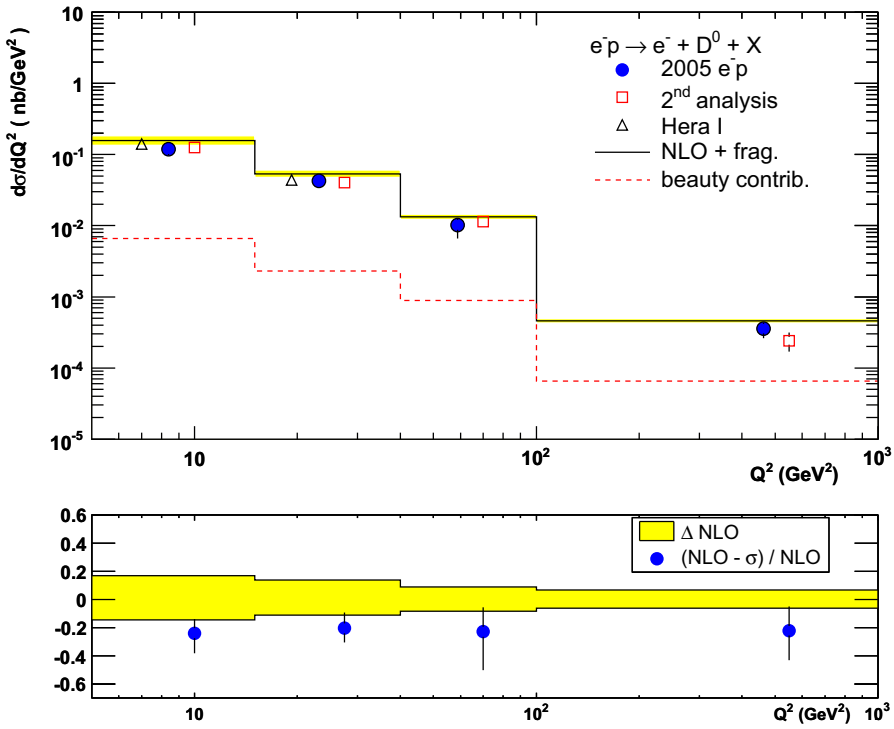

Figure 7.5. The differential cross-section $d\sigma/dQ^2$ for the process $e^-p \rightarrow e^- + D^0 + X$ was measured on a 2005 e^-p data sample of $127\,pb^{-1}$(top plot). The inner error bars (where visible) represent statistical errors, the outer bars denote the systematic errors. The results are compared to a second independent ZEUS measurement (only statistical error bars shown), to a measurement performed on Hera I data (the first 2 bins only) and to the NLO theoretical prediction. The beauty cross-section in the simulated files is also displayed, for reference. Bottom plot: the relative difference between the measurement and the NLO prediction is shown, together with its total error. The shaded band represents the error on the prediction.

ulated in Appendix B, Table B.2. The measurement is compared to the second independent analysis as well as to the NLO theoretical prediction. The beauty contribution to the cross-section, computed purely from the simulated sample, is also shown. The relative difference between the measurement and the NLO prediction is shown separately (bottom plot). The error bars correspond to the relative total error (statistical and systematic); the shaded band gives the relative error on the theoretical prediction. There is good agreement in shape but the measured cross-section values are $20 - 30\%$ lower. In the third P_T bin, the measurement agrees the least with the second analysis. The systematic errors on $d\sigma/dP_T(D^0)$ due to uncertainties in measuring the variables listed in Table 7.1 are displayed in Fig. 7.10, for each source independently. The total systematic error was obtained by

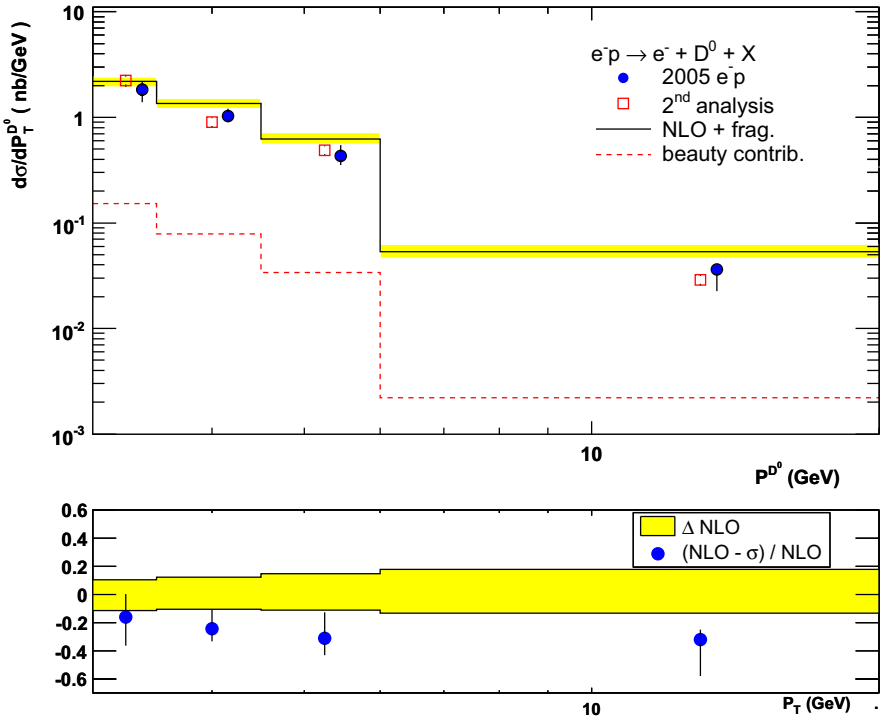

Figure 7.6. The differential cross-section $d\sigma/dP_T(D^0)$ for the process $e^-p \to e^- + D^0 + X$ was measured on a 2005 e^-p data sample of $127\,pb^{-1}$(top plot). The inner error bars (where visible) represent statistical errors, the outer bars denote the systematic errors. The results are compared to the second independent ZEUS measurement (only statistical errors shown) and to the next to leading order theoretical prediction. The beauty cross-section in the simulated files is also displayed, for reference. The relative difference between the measurement and the NLO prediction is shown separately (bottom plot). The error bars denote the relative total errors (statistical and systematic) whereas the shaded band is the relative error on the theoretical prediction.

adding the individual errors in quadrature. The measured cross-section has a large systematic error in the highest P_T bin due to the systematic error induced by the variation of D.L. significance.

7.3.3 Differential cross-section w.r.t. $\eta(D^0)$: $d\sigma/d\eta$

The differential cross-section as a function of the charmed meson pseudo-rapidity $\eta(D^0)$ for the process $e^-p \to e^- + D^0 + X$ has been measured for the following bins: $\eta \in [-1.6, -0.8, -0.4, 0, 0.4, 0.8, 1.6]$. The results are presented in Fig. 7.7 and tabulated in Appendix B, Table B.3. The measurement is compared to the second independent analysis as well as to the NLO theoretical prediction. The two

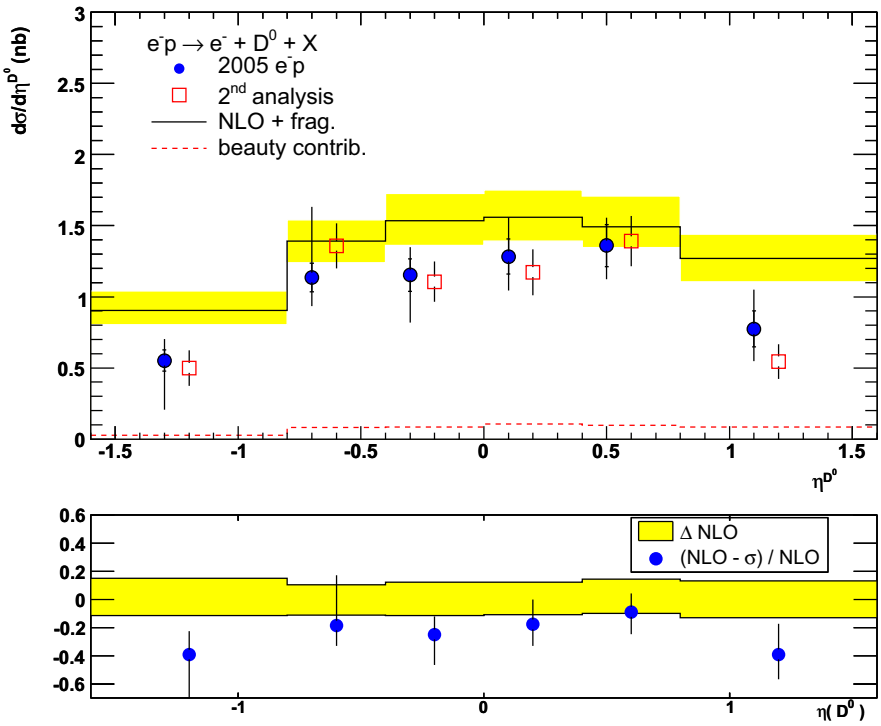

Figure 7.7. The differential cross-section $d\sigma/d\eta(D^0)$ for the process $e^-p \to e^- + D^0 + X$ was measured on a 2005 e^-p data sample of $127\,pb^{-1}$(top plot). The inner error bars represent statistical errors, the outer bars denote the systematic errors. The results are compared to the second independent ZEUS measurement (only statistical errors shown) and to the next to leading order theoretical prediction. The beauty cross-section in the simulated files is also displayed, for reference. The relative difference between the measurement and the prediction is shown separately (bottom plot). The shaded band represents the relative error on the NLO prediction whereas the error bars correspond to the relative total error.

analyses agree within the statistical errors. The beauty contribution to the cross-section, computed purely from the simulated sample, is also shown. The relative difference between the measurement and the NLO prediction is shown separately (bottom plot). Both the relative total errors on the measurement (error bars) and the error on the prediction (shaded band) are also displayed. The NLO calculation overestimates the cross-section by some $10 - 25\%$ in the central region and almost 40% at high and low η. The overall shape is reasonably reproduced. The systematic errors on $d\sigma/d\eta(D^0)$ due to uncertainties in measuring the variables listed in 7.1 are displayed in Fig. 7.11, for each source independently. The total systematic error was obtained by adding the individual errors in quadrature.

7.3.4 Differential cross-section w.r.t. Bjorken x: $d\sigma/dx$

The differential cross-section as a function of the Bjorken x ,for the process $e^-p \to e^- + D^0 + X$, has been measured for the following bins: $x \in \{10^{-4}, 5\times10^{-4}, 10^{-3}, 3.5\times10^{-3}, 10^{-1}\}$. The results are presented in Fig. 7.8 and tabulated in Appendix B, Table B.4 . The cross-section is concentrated at low values of x. The measurement

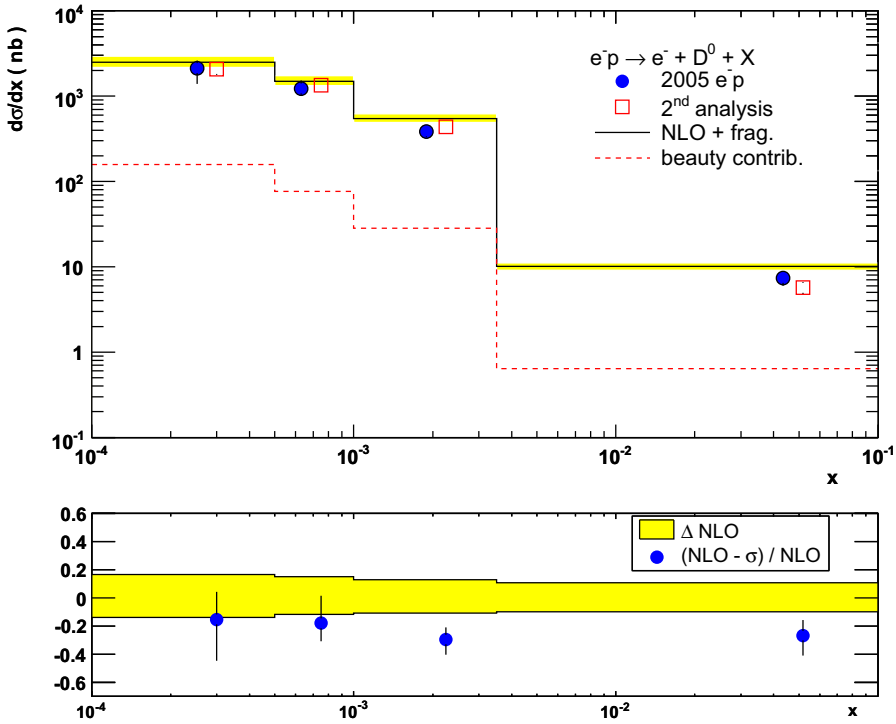

Figure 7.8. The differential cross-section $d\sigma/dx$ for the process $e^-p \to e^- + D^0 + X$ was measured on a 2005 e^-p data sample of $127\,pb^{-1}$(top plot). The inner error bars (where visible) represent statistical errors, the outer bars denote the systematic errors. The results are compared to the second independent ZEUS measurement (only statistical errors shown) and to the NLO theoretical prediction. The beauty cross-section in the simulated files is also displayed, for reference.The relative difference between the measurement and the prediction is shown separately (bottom plot). The shaded band represents the relative theoretical error whereas the error bars correspond to the relative total error on the measured cross-section.

is compared to the second analysis and to the next to leading order theoretical prediction. The beauty contribution to the cross-section, computed purely from the simulated sample, is also shown. The second analysis and the present analysis agree well, given the different tracking, vertexing and cut optimization used. The relative difference between the measurement and the theoretical prediction is displayed separately (bottom plot). A good agreement in shape with the NLO is seen but

the overall normalization is $15 - 30\%$ higher for the predicted cross-section. The systematic errors on $d\sigma/dx$ due to uncertainties in measuring the variables listed in 7.1 are displayed in Fig. 7.12, for each source independently. The total systematic error was obtained by adding the individual errors in quadrature.

7.4 The theoretical prediction

The theoretical predictions for the differential cross-sections, displayed in Fig. 7.5, 7.6, 7.7 and 7.8, were computed using the HVQDIS package [48]. HVQDIS calculates differential cross-sections of charm production in DIS in both leading order and next to leading order. Peterson fragmentation [49] is applied to both the charm and the anti-charm quarks at the hadron level. The Peterson fragmentation function depends only on one parameter, ϵ_P, determined by experiment [50]. Other inputs to HVQDIS are the renormalization and factorization scales μ_R and μ_F, the mass of the charm quark m_c and a particular choice of parton distribution functions. These input values together with their variations are given in Table 7.2.

Quantity	**Value**	**Variation**
Renormalization scale μ_R	$\mu_R = \sqrt{Q^2 + 4M_C^2}$	$2\sqrt{Q^2 + 4M_C^2}$
Factorization scale μ_F	$\mu_F = \mu_R$	larger of: $\frac{1}{2}\sqrt{Q^2 + 4M_C^2}$ or $2M_C$
Peterson parameter ϵ_P	0.035	± 0.030
Charm mass m_C	1.35 **GeV**	± 0.15 **GeV**
Input PDF's	ZEUS NLO PDF	ZEUS PDF: Upper and lower predictions

Table 7.2. The list of input parameters to the HVQDIS package used in calculating the central value. The input parameter variations are used to calculate the errors on the central value.

The differences between the measured (σ_{exp}) and theoretical (σ_{th}) differential cross-sections are quantified by $\delta\sigma_{rel}$:

$$\delta\sigma_{rel} = \frac{\sigma_{exp} - \sigma_{th.}}{\sigma_{th}} \tag{7.6}$$

$\delta\sigma_{rel}$ has been plotted as a function of Q^2, $P_T(D^0)$, $\eta(D^0)$, and Bjorken x in Fig. 7.5, 7.6, 7.7 and 7.8 respectively. The error bars on $\delta\sigma_{rel}$ denote both statistical

and systematic errors on the measurement, divided by the NLO central value. The relative error on the prediction is shown as a shaded band. The theoretical predicted cross-sections are on the average 20-30% higher than what the measurement finds. The relative difference is somewhat larger in η, where it reaches 40% at high and low η values.

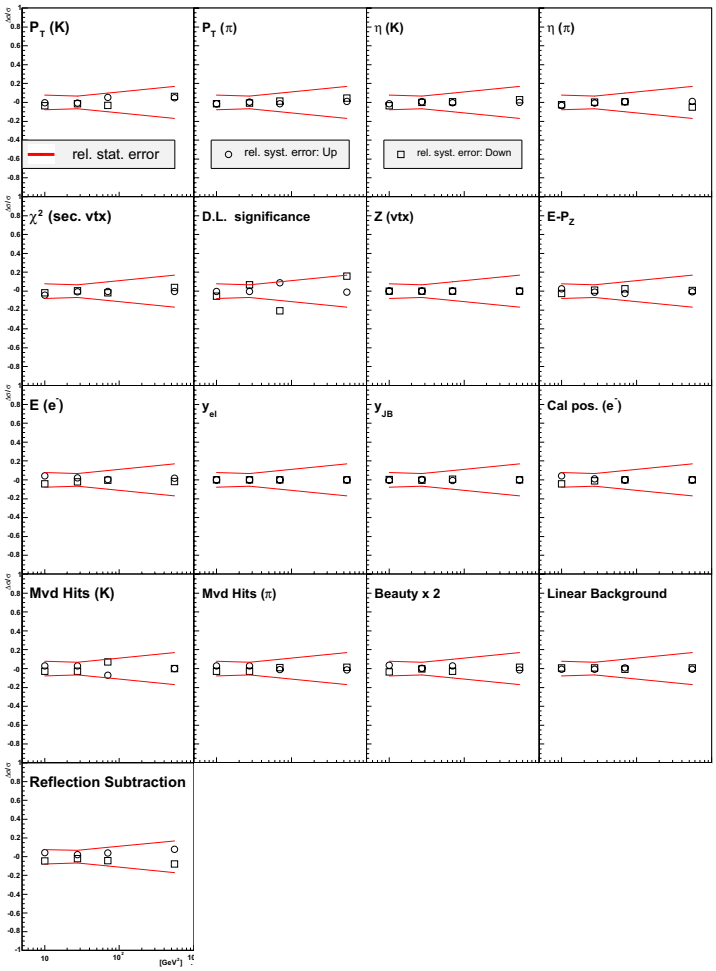

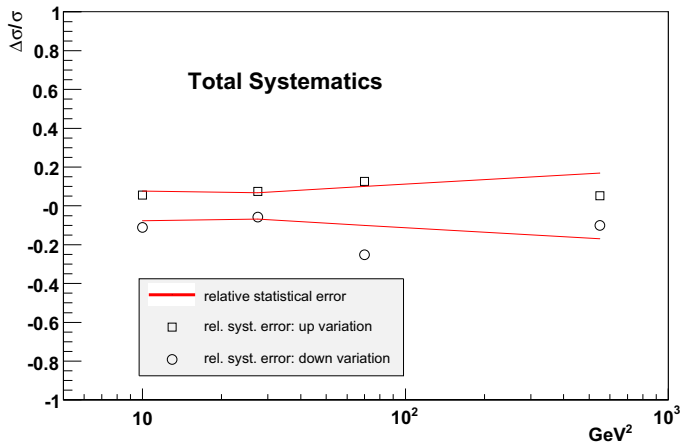

Figure 7.9. The systematic errors, calculated and labelled for each source separately, are displayed as a function of Q^2. A large contribution for all Q^2 bins comes from varying the decay length significance cut and from turning off the reflected signal subtraction. The total systematic error as a function of Q^2 (lower plot) is computed by adding in quadrature all systematic errors. The total systematic error is consistent with the statistical error.

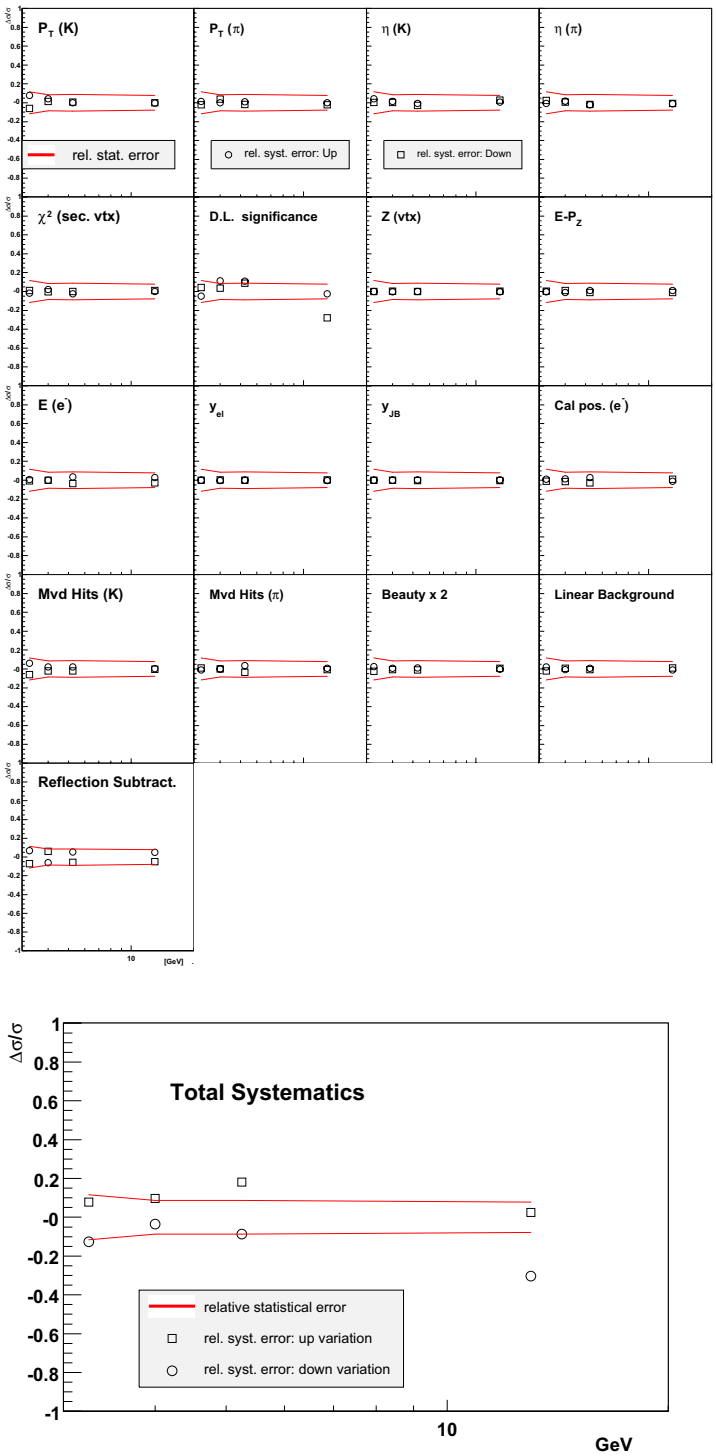

Figure 7.10. The systematic errors, calculated and labelled for each source separately, are displayed as a function of P_T of the charm meson. A large contribution for all P_T bins comes from varying the decay length significance cut and from turning off the reflected signal subtraction. The total systematic error as a function of P_T (lower plot) is computed by adding in quadrature all systematic errors. The total systematic error is consistent with the statistical error.

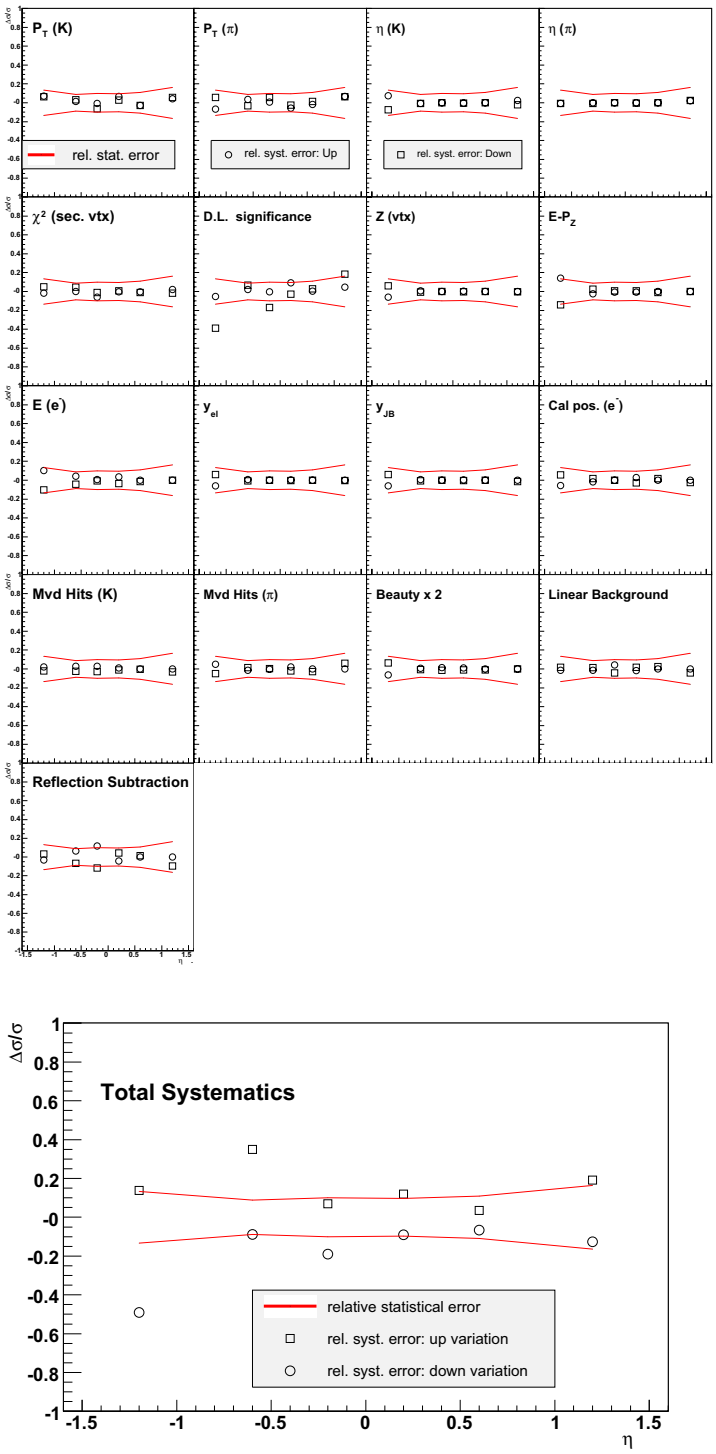

Figure 7.11. The systematic errors, calculated and labelled for each source separately, are displayed as a function of η of the charm meson. A large contribution for all η bins comes from varying the decay length significance cut and from turning off the reflected signal subtraction. The total systematic error as a function of η (lower plot) is computed by adding in quadrature all systematic errors. The total systematic error is consistent with the statistical error.

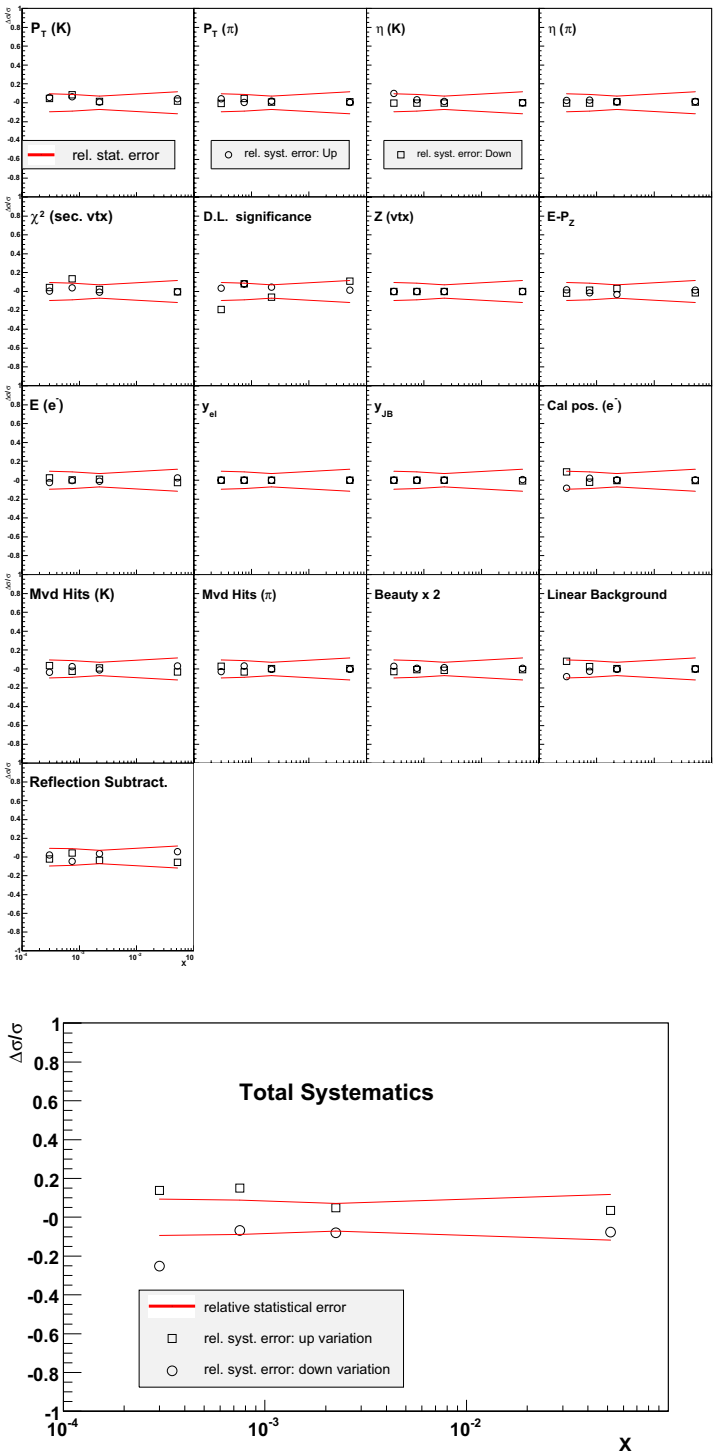

Figure 7.12. The systematic errors, calculated and labelled for each source separately, are displayed as a function of proton momentum fraction x of the struck quark. A large contribution for all x bins comes from varying the decay length significance cut and from turning off the reflected signal subtraction. At very low x, the systematic errors due to cuts on number of MVD hits and changing the background fit function become significant as well. The total systematic error as a function of x (lower plot) is computed by adding in quadrature all systematic errors. The total systematic error is consistent with the statistical error.